INTERNATIONAL JOURNAL OF ELECTRONICS, MECHANICAL and MECHATRONICS ENGINEERING
Vol.2 Num.1 pp.(110-127)

AUTOMATIC ISOCONTOUR DETERMINATION FOR IODINE DOSE CALCULATION USING CELLULAR NEURAL NETWORKS ON SCINTIGRAPHIC IMAGES

Roger Lédée[1] Fabien Courrèges[1] Rachid Harba[1] Onur Osman[2] Osman N.Ucan[3*]

[1]University of Orléans, BP 6744, 12 Rue de Blois, 45067, Orléans Cedex 2, France

[2]Istanbul Arel University, Engineering Faculty, Electronics Eng. Dept. Istanbul

[3*]Istanbul Aydin University, Engineering-Architecture Fac. Electrical and Electronics Dept.

Florya , Istanbul, Turkey (*Corresponding author) uosman@aydin.edu.tr

ABSTRACT

The hyperthyroid disease treatment consists in swallowing iodine 131. The quantity of these radio isotope results in an evaluation of the thyroid volume from a single scintigraphic image. In medical routine, the volume is calculated from a manual selection of an isocontour defining the boundary of the thyroid. We propose in this paper an automatic method to extract this boundary using Cellular Neural Network (CNN). Results show that our method is comparable to manual choice given by four experts. Studied on 35 patients with hyperthyroid diseases, we conclude that CNN is a comprising approach in segmentation of scintigraphic images.

Keywords: Thyroid, radioiodine, scintigraphy, cellular neural networks, isocontour

AUTOMATIC ISOCONTOUR DETERMINATION FOR IODINE DOSE CALCULATION USING CELLULAR NEURAL NETWORKS ON SCINTIGRAPHIC IMAGES

(Roger Lédée Fabien Courrèges Rachid Harba Onur Osman Osman N.Ucan)

1. INTRODUCTION

The treatment by radioiodine ^{131}I (iodine 131) is effective to treat different thyroid disorders. ^{131}I constitutes a reasonable therapeutic alternative, in cases with absolute or relative contraindication for surgery [1]. To calculate the dose to be administrated as therapy, it is necessary first to determine the volume of thyroid that will uptake ^{131}I. In obtaining thyroidal volumes, there are two main techniques. These are ultrasonography (US) and scintigraphy (SC). In US, anatomic volume can be determined. Where else, in SC only the volume that absorbs iodine is regarded. Thus SC is preferable to US. But in SC, 2D images are obtained by low dose ^{131}I, resulting low resolution and noise. The acquisition process lasts more than fifteen minutes and the resulting image is dependant on movements of the patients.

To determine the thyroidal volume, it is necessary to extract an isocontour defining the boundary of the part of the thyroid fixing iodine. Then surface, volume, mass and dose for the treatment are calculated with existing formulas and models: the estimation of thyroidal volume is calculated by an ellipsoidal model or the formulation suggested by Himanka and Larsson in 1955 [2]. In SC current practice, isocontour is chosen by manually selecting a threshold or by setting a lower threshold such as 20% of the maximum of grey level [3-5]. This approach may cause subjective results and give a low inter and intra observer reproducibility. To remedy this drawback we aim at developing an automatic algorithm able to perform the task of delineating the surface of interest in a SC image.

For the delineation of the structures in an image, there are many algorithms called image segmentation algorithms. And, it's difficult to choose a method to obtain the best segmentation. Currents methods used for computer assisted or computer automated segmentation of anatomical medical images are described in a review suggested by Pham, Xu and Prince [6]. But, for functional medical images as SC, few segmentation methods are adaptable. Recent works use a fuzzy logic technique for segmenting dynamic neuroreceptor in single-photon emission tomography images [7] or for locating abnormalities in bone scintigraphy [8]. Several artificial neural networks (ANN) have been developed for the diagnosis of pulmonary embolism from perfusion-ventilation scans [9-13]. These studies show that the systems containing ANN are an independent and an additional device for supporting doctor's diagnosis. The difficulties are on the choice of the structure of the ANN and on the research of the most optimal parameters. In image processing, to guide the choice of the type of neural networks and of future perspectives, Egmont-Petersen, de Ridder and Handels in [14] review more than 200 applications of neural networks and present a novel two-dimensional taxonomy.

In SC current practice, experts exploit spatial information around the boundary of the active zone to select a threshold. So, we propose to exploit a neural network functioning on the same principle. The aim of this study is to implement and test a data processing method based on Cellular Neural Networks (CNN) to estimate the level of an isocontour automatically. A CNN is a system in which nodes are locally connected. Each node contains a feedback template and a control template that contain few parameters to be determined. Then surface, volume, mass of thyroid and intake iodine dose can be calculated objectively. We also aim to minimize errors occurred by human factors.

This paper is organized as follows. In Section 2, Cellular Neural Network is explained and applied to SC data. In section 3, results are given for different cases. Finally, section 4 concludes the paper.

2. MATERIALS AND METHODS

We have obtained 35 images of patients having thyroid problem from Nuclear Medicine Department of the Regional Hospital Centre of Orléans (CHRO) in France and each image is evaluated by four different experts coded as {A,B,C,D}. The age of patients (29 women and 6 men) are between 30 to 88 years old with a mean of 57.4. All data were acquired with a scintillation probe (gamma camera GKS2 produced by GAEDE) 24h after ingestion of a capsule containing 1.85 MBq ^{131}I-NaI. The gamma camera was positioned at the site of the patient's thyroid area at an average distance of 5 cm. Acquisitions parameters are: anterior view, 128*128 matrix, pixel size 0.136 cm, acquisition time 900 s.

In evaluation of thyroidal images, isocontour estimation is vital and in practice it's chosen by manually selecting a threshold or by setting a lower threshold such as 20% of the maximum of grey level [3-5], [15]. In this paper, we propose an automatically detection of isocontours using Cellular Neural Networks (CNN). Generally, Neural Networks fall into two main classes: (1) memory less Neural Networks and (2) dynamical Neural Networks. Memory-less Neural Networks have been used for simple static problems. But dynamic models such as in Hopfield Networks (HN) and Cellular Neural Networks (CNN), neural networks have usually been designed as dynamical systems where the inputs are set to some constant values and each trajectory approaches one of the stable equilibrium points depending upon the initial state. CNN is a dynamic large-scale non-linear analog circuit which processes signals in real time [16]. Like cellular automata, it is made of massive aggregate of regularly spaced circuits clones, called cells, which communicate with each other directly only through its nearest neighbors (Figure 1). The adjacent cells can interact directly with each other. Cells not directly connected together may affect each other indirectly because of the propagation effects of the continuous-time dynamics of cellular neural networks. An example of a two-dimensional CNN is shown in Figure 2. We call the cell on the i^{th} row and j^{th} column cell C*(i,j)* as in Figure 2. Now let us define, neighborhood of C*(i,j)*.

Definition: r-neighborhood
The r-neighborhood of a cell C*(i,j)* , in a cellular neural network is defined by,

$$N_r(i,j) = \left\{ C(k,1) \middle| \max\left\{ |k-i|, |1-j| \right\} \le r \right\}$$
$$1 \le k \le M; 1 \le 1 \le N \qquad (1)$$

where, r is a positive integer number. Figure 2 shows neighborhoods of the C(i,j) cell (located at the center and shaded) with r = 1, 2 and 3, respectively. Cells are multiple input-single output nonlinear processors all described by one or one among several different, parametric functional. A cell is characterized by a state variable that is generally not observable as such outside the cell itself. It contains linear and non-linear circuit elements such as linear resistors, capacitors and non-linear controlled sources. Every cell is connected to other cells within a

$$\frac{dx_{ij}(t)}{dt} = \sum -x_{ij}(t) + \sum_{kl \in N_r(ij)} A_{(i-k)(j-l)}(t) y_{kl} + \sum_{kl \in N_r(ij)} B_{(i-k)(j-l)}(t) u_{kl} + I \tag{2}$$

$$y_{ij}(t) = f\left[x_{ij}(t)\right] = \frac{1}{2}\left(\left|x_{ij}(t)+1\right| - \left|x_{ij}(t)-1\right|\right) \tag{3}$$

where x, y, u, I denote respectively cell state, output, input, and bias; j and k cell indices. CNN parameter values are assumed to be spaced-invariant and the nonlinear faction is chosen as piece-wise linear. A, B and I are cloning template matrices are identically repeated in the neighborhood of every neuron as,

$$A = \begin{bmatrix} A_{-1,1} & A_{-1,0} & A_{-1,1} \\ A_{0,-1} & A_{0,0} & A_{0,1} \\ A_{1,-1} & A_{1,0} & A_{1,1} \end{bmatrix}, \quad B = \begin{bmatrix} B_{-1,1} & B_{-1,0} & B_{-1,1} \\ B_{0,-1} & B_{0,0} & B_{0,1} \\ B_{1,-1} & B_{1,0} & B_{1,1} \end{bmatrix}, I \tag{4}$$

The network behavior of CNN depends on the initial state of the cells activation, namely bias I and on weights values of A and B matrices which are neighborhood of itself. In this scheme, information is only exchanged between neighboring neurons and this local information characteristic does not prevent the capability of obtaining global processing. The CNN is a dynamical system operating in continuous or discrete time. A general form of the cell dynamical equations may be stated as follows:
associated with the connections inside the well-defined neighborhood of each cell. CNN's are arrays of locally and regularly interconnected neurons, or, cells, whose global functionality are defined by a small number of parameters (A, B, I) that specify the operation of the component cells as well as the connection weights between them. CNN can also be considered as a nonlinear convolution with the template. Since we use discrete 2-D images (medical in this case or for another modality [17]), Equation (2-3) will be rewritten as:

$$x_{ij}(n+1) = -x_{ij}(n) + \sum_{kl \in N_r(ij)} A_{(i-k)(j-l)}(n) y_{kl} + \sum_{kl \in N_r(ij)} B_{(i-k)(j-l)}(n) u_{kl} + I \tag{5}$$

$$y_{ij}(n) = f\left[x_{ij}(n)\right] = \frac{1}{2}\left(\left|x_{ij}(n)+1\right| - \left|x_{ij}(n)-1\right|\right) \tag{6}$$

Since their introduction in 1988, Cellular Neural Network has attracted a lot of attention [18]. Not only from a theoretical point of view these systems have a number of attractive properties, but furthermore there are many well-known applications like image processing, motion detection, pattern recognition, simulation. Here we have applied this contemporary approach for isocontour estimation of real data. The reduced numbers of connections within a local neighborhood, the principle of cloning template etc., turn out to be advantage of CNN's (Figures 1-2).

A. Learning algorithm

In CNN, we have to train A, B, I templates using various optimization methods to solve the problem of border detection of synthetic and real data. Here, we have optimized weight coefficients of A, B matrices and bias I of synthetic examples using recurrent perceptron learning algorithm (RPLA) defined by [19]. RPLA optimization criterion is as follows:

$$\varepsilon[w] \equiv \sum_{s=1}^{N} \varepsilon'^{s}[w] = \sum_{s} \sum_{i,j} (y_{i,j}^{s}(\infty) - d_{i,j}^{s})^2 \quad (7)$$

where $y^s_{i,j}(\infty)$ is the steady state of output at s^{th} input vector, $d^s_{i,j}$ is the desired sequence and $\varepsilon[w]$ is the total error that will be minimized. The RPLA can be described as the following set of rules:

i) Increase each feedback template coefficient, which defines the connection to a mismatching cell from its neighbor whose steady state output is same with the cell's desired output. On the contrary, decrease each feedback template coefficient, which defines the connection to a mismatching cell from its neighbor whose steady state is different from the cell's desired output.

ii) Change the input template coefficients according to the rule stated in (i) by only replacing the word of neighbor with input.

iii) Retain the template coefficients unchanged if the actually outputs match the desired outputs.

B. APPLICATION OF CNN TO THYROIDAL IMAGES

We have obtained 35 images of patients having thyroid problem from CHRO and each image is evaluated by four different experts. We have used 18 of them in training and the rest for testing CNN results. We have trained CNN regarding the isocontour values selected by four experts {A, B, C, D} as shown in Table I.

In order to estimate optimum isocontour of thyroid image, two level procedures are applied as illustrated in figure 3. At the first level processing, a de-noising and smoothing is achieved by a simple but efficient convolution filter. We have chosen the filter's mask according to the following consideration: the effect of the transfert function of the acquisition system (gamma camera) leads us to admit the hypothethis that the signal image is locally quasi-stationary. It is known that scintigraphic images are affected by Poisson noise [20]. That's why the choice of an averaging filter enables to compute the maximum likelihood estimator. Because of the low resolution of the images (a pixel is mapped to an area of 0.136 x 0.136 cm^2) we have chosen a 3x3 mask filter, in order to avoid too much smoothing and the loss of details. Thus the mask filter is chosen as:

$$LP = \frac{1}{9}\begin{bmatrix} 1 & 1 & 1 \\ 1 & 1 & 1 \\ 1 & 1 & 1 \end{bmatrix} \quad (8)$$

The performance of this filter on synthetic phantom image artificially corrupted by Poisson noise, gives an improvement of more than 10 dB on the Peak Signal to Noise Ration (PSNR). Figure 4 shows the filtering effect on a thyroid scintigram like phantom (with nodules). The Poisson noise process is simulated so that to obtain a total of about 2.5x105 counts in the noisy image. This number of counts corresponds to the common count values of the images acquired in medical routine. It can also be proven that under the assumption of quasi-stationnarity, the averaging filter maximises the signal to noise ratio when the image is degraded by Poison noise (see demonstration in annexe).

Then pre-processed image is analyzed by CNN as a second level of processing. The first stage of this second level CNN process, involves estimation of A, B and I template coefficients using the RPLA algorithm. At this stage, a part of data set is used for learning. This stage is where the weighting coefficients are determined. Then CNN template coefficients are found as:

$$A = \begin{bmatrix} 0 & 0 & 0 \\ 0 & 1.03 & 0 \\ 0 & 0 & 0 \end{bmatrix}, B = \begin{bmatrix} -1.01 & -0.98 & -1.01 \\ -0.98 & 7.99 & -0.98 \\ -1.01 & -0.98 & -1.01 \end{bmatrix}, \mathrm{I} = -1 \quad (9)$$

After the learning stage is completed, next stage involves the testing, where isocontour detection/segmentation performance of CNN is evaluated. At this stage, weight coefficients of A, B and I templates, which are determined in Equation (9), are used to obtain test outputs. In testing, we evaluate 4 x 17 of the data set of patients coded as {1 to 35}. We check our CNN outputs with experts' results and perfect matching is found. As example sets, we have chosen some specific samples of patients as shown in Figure 5-8. The results confirmed that CNN may be a powerful tool in scintigraphic segmentation process. CNN is capable of estimation of contours automatically. Thus region of interest is found including the entire thyroid gland and leaving out all non-thyroidal radioactivity concentrations, most notably the salivary glands. In the mean time, human subjectivity is minimized while evaluating raw image.

After optimal isocontours are estimated by CNN, it is necessary to calculate related values such as surface, volume, mass and activity which will help the experts to give necessary amount of intake to the patients. Thus we have first calculated Surface (cm^2), as a summation of pixels in thyroidal region. In CHRO, each pixel is mapped to an area of (0.136 x 0.136) cm^2 as a result of the resolution in technical equipments.

In a scintigraphic study of largely varying thyroid sizes and conditions, Himanka and Larsson found that the frontal projection was the sole of variable determining thyroid volume [2]. Then Volume (cm^3), Mass (g) and iodine intake in Mega Becquerel (MBq) values are calculated as,

$$Volume = \frac{1}{3} S^{3/2} \quad (10)$$

Here, Surface (S) is calculated by summation of pixels that take place in the inner section of the isocontour, we express as thyroidal region and multiplied by a resolution dependent constant (0.136 x 0.136). This formula was derived experimentally through determination of volumes of surgical thyroid specimens by fluid replacements [2]. The other related parameter is the mass of the thyroidal region which can be calculated as,

$$Mass = Volume * \rho \tag{11}$$

where, ρ is volumetric mass. Here it is chosen as 1.025. Activity (A) in Mega Becquerel (MBq), is also calculated using Equations (10-11) as,

$$A = \frac{23.4 * Mass * D}{5 * T} \tag{12}$$

where, D is chosen as 80 in Gray and T is defined as fixation ratio measured on patients, 24 hours passed after radioiodine uptake for realization of scintigraphy. Activity A is calculated to achieve therapy to patients with thyroidal disease [15]. The therapeutic ^{131}I dose (directed at 4.4 MBq ml^{-1} thyroid tissues) is calculated using the formula,

$$^{131}I \text{ dose (MBq)} = \frac{4.4\,(\text{MBq ml}^{-1}) * 100}{24 \text{ uptake } (\%) * \text{V (ml)}} \tag{13}$$

In our case, isocontours values of hyperthyroid patients are obtained by CNN and related parameters are calculated by Equations (10-12). The results are compared with expert radiologists' in Table I. The experts choose any isocontour value manually regarding his/her experience and all other parameters are calculated upon this manually selected main parameter. Four different experts have evaluated the same raw data after selection their own isocontour values. There seems to be variation even such a small group of experts. The selection of isocontour is vital, since radioiodine uptake, A is calculated as in Equations (10-12) depending on isocontour parameter. In CNN, isocontour is automatically selected regarding the neighborhood of pixels and over all global optimization of the raw image. Using isocontour ratios and calculated related parameters {surface and mass, iodine intake values} for CNN outputs and experts' manual operation are listed in Table I. Thyroid fixation, last column of the Table, is the iodine amount remained in thyroids in 24hours following first iodine is injected/taken. As shown in Equation (12) and in Figure 13, in calculation, activity A, fixation value is also a parameter.

3. RESULTS

In this paper, we aim to estimate isocontours of 2-D thyroidal images automatically, to optimize objectivity criteria and to calculate dose of radioiodine treatment of each individual patient, using Cellular Neural Network (CNN) approach. We study on 35 patients in CHRO. We detect isocontour values of thyroidal images by CNN automatically and improve patients' health care. We have listed CNN and experts' results in Table I and compare each parameter in Figure (5-12). In Figure (5-7), we select some cases to represent the performance of CNN regarding the classical results. We have also drawn all calculated parameters {Surface (cm^2), Volume (cm^3), Mass (g) and iodine intake in Mega Becquerel (MBq)} and compared with CNN outputs in Figures (9-12). CNN has similar results with experts' results. In Figure 13, fixed thyroid (T) is drawn for each patient.

4. CONCLUSION

In thyroidal diseases, the therapy aim and the preferred dosage strategy of radioiodine treatment evidently vary not only with the thyroid disorders that are to be cured, but also from country to country or even from clinic to clinic. So individualized treatment protocols are the most appropriate way to improve the success of radioiodine therapy. In this paper, as patient-tailored radioiodine therapy, we aim to estimate isocontours of 2-D thyroidal images automatically, to optimize objectivity criteria and to calculate dose of radioiodine treatment of each individual patient, using Cellular Neural Network (CNN) approach. We study on 35 patients with hyperthyroid diseases in Regional Hospital Centre of Orléans (CHRO). The age of patients (29 women and 6 men) are between 30 to 88 years old with a mean of 57.4. CNN is a supervised, space invariant 2-Dimensional image processing technique. Each CNN cell is composed of three cascaded blocks, first block works as a summation of input data and CNN feedback, second block represents dynamic property of CNN system and the last block is a piece-wise linear filter. CNN has been applied to various areas such as texture analyzing, de-noising, clustering, potential anomaly separation etc. since its introduction in 1988 by Leon Chua. Since we estimate isocontour values of thyroidal images by CNN automatically in an objective style, we increase patients' health care. We have listed CNN and experts' results in Table I and compare each parameter in Figure (5-12). We have obtained satisfactory results by CNN. Thus, we conclude that CNN is a comprising approach in segmentation of scintigraphic images.

ANNEXE

Let us demonstrate that the power signal to noise ratio is maximised when using an averaging filter on Poisson data. We adopt the following notations : be *s* the image signal to be restored, be *b* the additive noise signal affecting the image, and be *y* the measured image. We consider the model: y = s + b

We note as well $\aleph_N(i)$ the set of indices of the NxN neighbouring pixels of pixel i. Our objective is to compute the NxN convolution filter h allowing the maximisation of the power signal to noise ratio K_i pour each pixel i of the image.

$$K_i = \frac{\left|(s*h)_i\right|^2}{E\left(\left|(b*h)_i\right|^2\right)} \tag{A1}$$

Where E(.) denotes the expectation operator.

By discretising the previous equation, we obtain:

$$K_i = \frac{\sum_{j\in\aleph_N(i)} \sum_{j\in\aleph_N(i)} h_j h_k s_j s_k}{\sum_{j\in\aleph_N(i)} \sum_{k\in\aleph_N(i)} h_j h_k E\left(b_j b_k\right)} \tag{A2}$$

The measured image is supposed to be generated from a Poisson process leading to a Poisson conditional probability model for each pixel i:

$$P(y_i|s_i) = \frac{s_i^{y_i} e^{-s_i}}{y_i!} \quad \text{(A3)}$$

with the proprieties : $E(y_i) = s_i$ and $Var(y_i) = s_i$, where Var(.) is the variance operator.
Hence we can derive the noise probability:

$$P(b_i|s_i) = P((s_i + b_i)|s_i) = \frac{s_i^{s_i+b_i} e^{-s_i}}{(s_i + b_i)!} \quad \text{(A4)}$$

We easily verify that $E(b_i) = 0 \ \forall$ i and for every s_i. We also have the propriety $Var(b_i) = E(b_i^2) = s_i$.
We know need the independence hypothethis: the noise is supposed to be independent for each pixel. This leads to the relation: $E(b_i b_j) = E(b_i)E(b_j) \ \forall \ i \neq j$.
As $E(b_i) = 0$ we have $E(b_i b_j) = 0 \quad \forall \ i \neq j$.

With these results we rewrite K_i as:

$$K_i = \frac{\sum_{j\in\aleph_N(i)} \sum_{j\in\aleph_N(i)} h_j h_k s_j s_k}{\sum_{j\in\aleph_N(i)} h_j^2 E\left(b_j^2\right)} = \frac{\sum_{j\in\aleph_N(i)} \sum_{j\in\aleph_N(i)} h_j h_k s_j s_k}{\sum_{j\in\aleph_N(i)} h_j^2 s_j} \quad \text{(A5)}$$

To guarantee the conservation of the local mean in the image, the mask filter has to be normalised as: $\sum_{i=1}^{N} h_i = 1$
Then with these elements let us show that K_i is maximum when every h_i are equals. We differentiate K_i with respect to an element h_ℓ of h:

$$\frac{\partial K_i}{\partial h_\ell} = \frac{2s_\ell \sum_j h_j s_j \sum_j h_j^2 s_j - 2h_\ell s_\ell \left(\sum_j h_j s_j\right)^2}{\left(\sum_j h_j^2 s_j\right)^2} \quad \text{(A6)}$$

$$\frac{\partial K_i}{\partial h_\ell} = 0 \iff \sum_j h_j^2 s_j - h_\ell \sum_j h_j s_j = 0 \iff \sum_j \left(h_j^2 - h_\ell h_j\right) s_j = 0 \quad \text{(A7)}$$

The choice $h_\ell = h_j$ provides a stationary point and by absurd reasoning it can easily be shown that:

$$K_i \leq \frac{\sum_{j\in\aleph_N(i)} \sum_{k\in\aleph_N(i)} s_j s_k}{\sum_{j\in\aleph_N(i)} s_j} = \sum_{j\in\aleph_N(i)} s_j \quad \text{(A8)}$$

ACKNOWLEDGEMENT
The authors gratefully acknowledge M.T. Guilhem, S. Gauvain and the other doctors (Hospital of Orléans, France) for gathering raw data of thyroid patients and their analyses.

REFERENCES:

1. F.L. Velayoudom, X. Marchandise, M. Nocaudie, M. d'Herbomez, C. Docao, C. Bauters, F. Regnier, J.L. Wemeau, 131 iodine for the treatment of benign goiters, *Presse Med.* 34 (2005) 94-100.

2. E. Himanka, L.G. Larsson, Estimation of thyroid volume, Acta Radiol. 43 (1955) 125-131.
3. M.F.T. Wesche, M.M. Tiel-v.Buul, N.J. Smits, W.M. Wiersinga, Ultrasonographic versus scintigraphic measurement of thyroid volume in patients referred for 131I therapy, Nuclear Medicine Communications 19 (1998) 341-346.
4. Johanne Willem, Dosage assessment for radioiodine therapy in benign thyroid disorders, PhD thesis of the University Medical Center Utrecht, The Netherlands, 2001.
5. G.S. Pant, R. Kumar, A.K. Gupta, S.K. Sharma, A.K. Pandet, Estimation of thyroid mass in Graves'disease by scintigraphic method, Nuclear Medicine Communications 24(7) (2003) 743-748.
6. D.L. Pham, C. Xu, J.L. Prince, A survey of current methods in medical image segmentation, *Annual Review of Biomedical Engineering* 2 (2000) 315-337.
7. P.D. Acton, L.S. Pilowsky, H.F. Kung, and P.J. Ell, Automatic segmentation of dynamic neuroreceptor single-photon emission tomography images using fuzzy clustering, *Eur. J. Nucl. Med.* 26(6) (1999) 581-590.
8. T-K. Yin, N-T. Chiu, A computer-aided diagnosis for locating abnormalities in bone scintigaphy by a fuzzy system with a three-step minimization approach, *IEEE Transactions on Medical Imaging* 23(5) (2004) 639-654.
9. J.A. Scott, E.L. Palmer, A.J. Fischman, How well can radiologists using neural network software diagnose pulmonary embolism?, *A. J. R.* 175 (2000) 399-405.
10. H. Holst, K. Mare, A. Jarund, et al., An independent evaluation of a new method for automated interpretation of lung scintigrams using artificial neural networks, *Eur. J. Nucl. Med.* 28 (2001) 33-38.
11. Eng J., Predicting the presence of acute pulmonary embolism: a comparative analysis of the artificial neural network, logistic regression, and threshold models, *A. J. R.* 179 (2002) 869-874.
12. G. Serpen, R. Iyer, H. M. Elsamaloty and E. I. Parsai, Automated lung outline reconstruction in ventilation–perfusion scans using principal component analysis techniques, *Computers in Biology and Medicine* 33 (2003) 119-142.
13. D. Swietlik, T. Bandurski, P. Lass, Artificial neural networks in nuclear medicine, *Nucl. Med. Rev. Cent. East Eur.* 7(1) (2004) 59-67.
14. M. Egmont-Petersen, D. de Ridder, H. Handels, Image processing with neural networks – a review, *Pattern Recognition* 35(10) (2002) 2279-2301.
15. L.B. Rasmussen, L. Ovesen, I. Bülow, T. Jorgensen, N. Knudsen, P. Laurberg, H. Perrild, Relations between various measures of iodine intake and thyroid volume, thyroid nodularity and serum thyroglobulin, *Am. J. Clin. Nutr.* 76 (2002)1069-1076.
16. L.O. Chua, L. Yang, Cellular Neural Networks: Application, *IEEE Transactions on Circuits and Systems* 35(10) (1998) 1273-1290.

17. A.M. Albora, O.N. Ucan, A. Ozmen A. and T. Ozkan, Separation of Bouguer anomaly map using cellular neural network, *Journal of Applied Geophysics* 46(2) (2001) 129-142.

18. V. Cimagalli, Cellular Neural Networks: A Review, *Proceedings of sixth Italian workshop on parallel architectures and Neural Networks*. Vietri Sul Mare, Italy, May 12-14 (1993).

19. C. Guzelis, S. Karamahmut, Recurrent perceptron learning algorithm for completely stable Cellular Neural Networks, *Proc. Third IEEE Int. Workshop on Cellular Neural Network and Applications*, Rome, Italy, (1994)177-182.

20. K.K. Shung, M.B. Smith, and B. Tsui, Principles of medical imaging, *Academic Press*, (1992).

FIGURES:

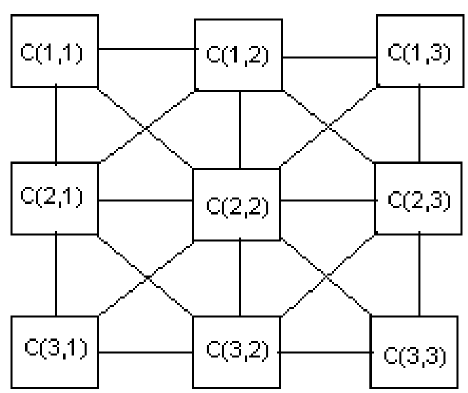

Figure 1. 2-D CNN Structure

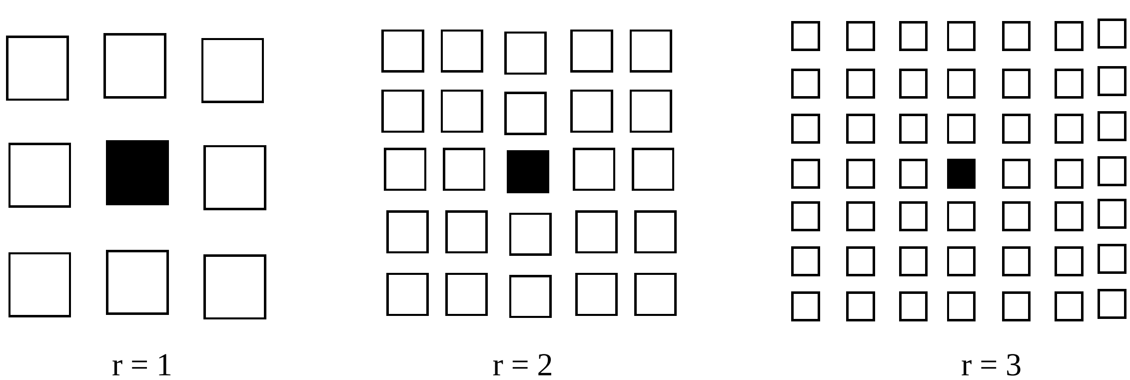

Figure 2. Various neighborhood models of CNN structure

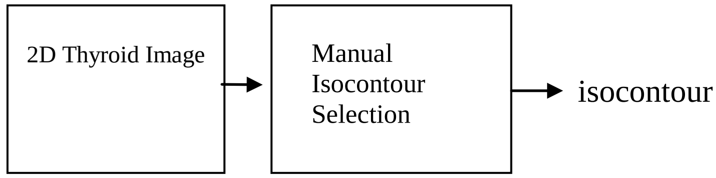

(a)

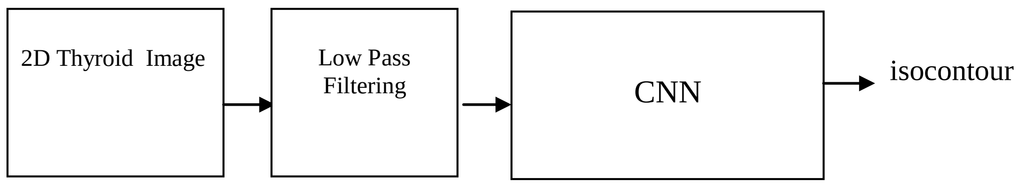

(b)

Figure 3. Block diagram of isocontour selection (a) classical manual selection (b) CNN approach

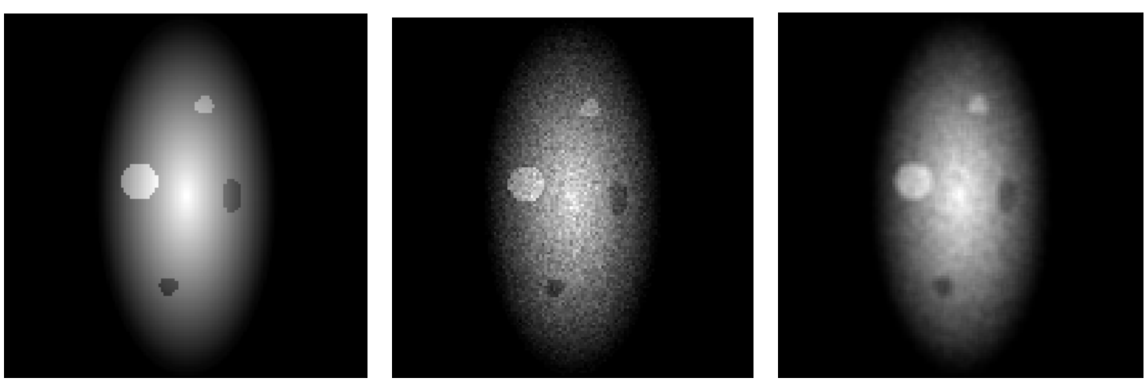

(a) (b) (c)

Figure 4. (a) Original 128x128 pixels synthetic phantom image.
(b) Poisson noise degraded image (image intensities are scaled for visibility), PSNR= 22.85 dB.
-c- Filtered image with an averaging 3x3 mask, PSNR = 31.22 dB

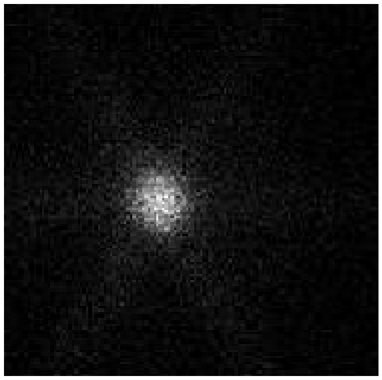

(a)

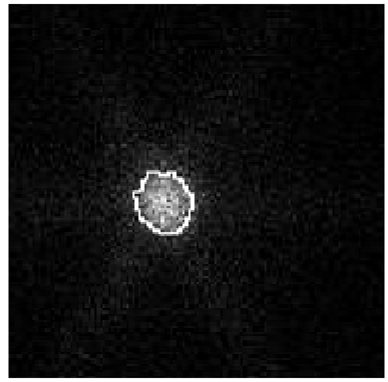

(b)

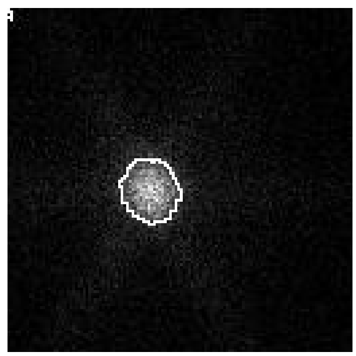

(c)

Figure 5. Performance of CNN scheme for one lobe thyroid image of Patient No.20: (a) 2D Input Image (b) CNN output (c) Result of Expert {A}

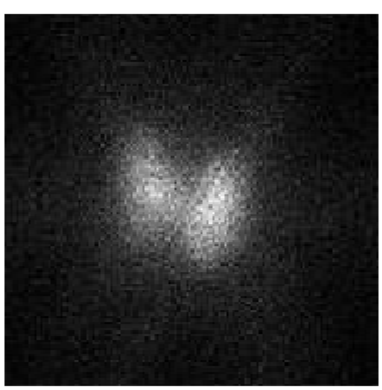

(a)

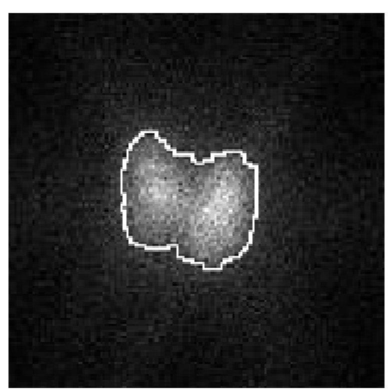

(b)

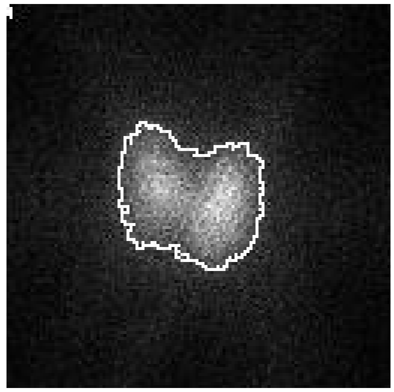

(c)

Figure 6. Performance of CNN scheme for two lobe thyroidal images of Patient No.01: (a) 2D Input Image (b) CNN output (c) Result of Expert {A}

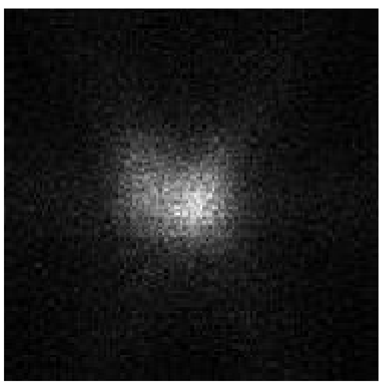

(a)

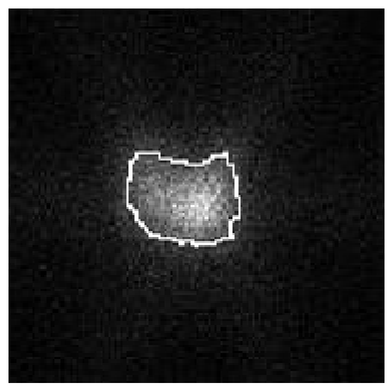

(b)

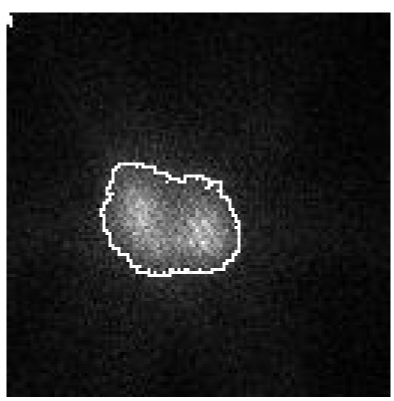

(c)

Figure 7. Performance of CNN scheme for combined lobes of thyroidal images of Patient No.03: (a) 2D Input Image (b) CNN output (c) Result of Expert {A}

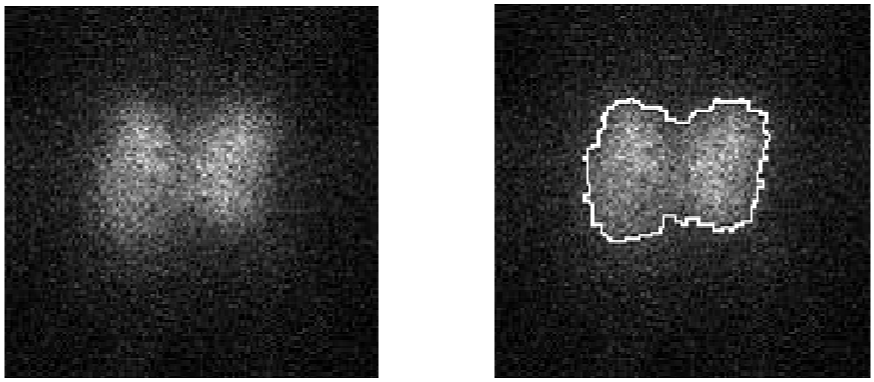

(a) (b)

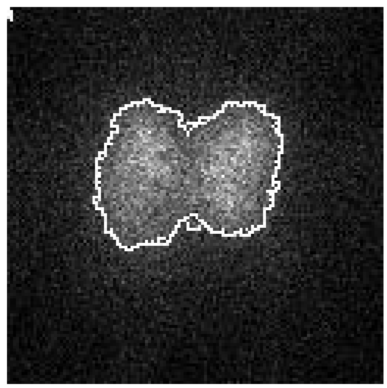

(c)

Figure 8. Performance of CNN scheme for separate lobes of thyroidal images of Patient No.06: (a) 2D Input Image (b) CNN output (c) Result of Expert {A}

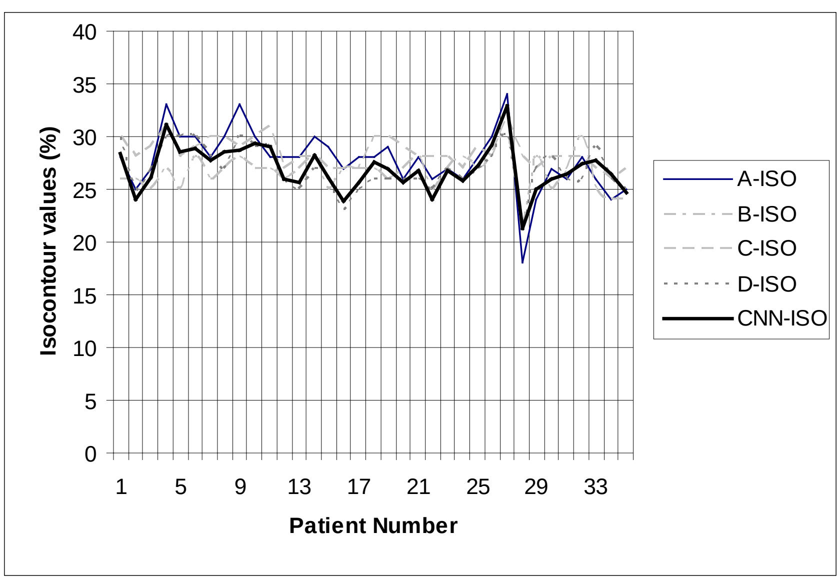

Figure 9. Isocontours of experts {A,B,C,D}and CNN

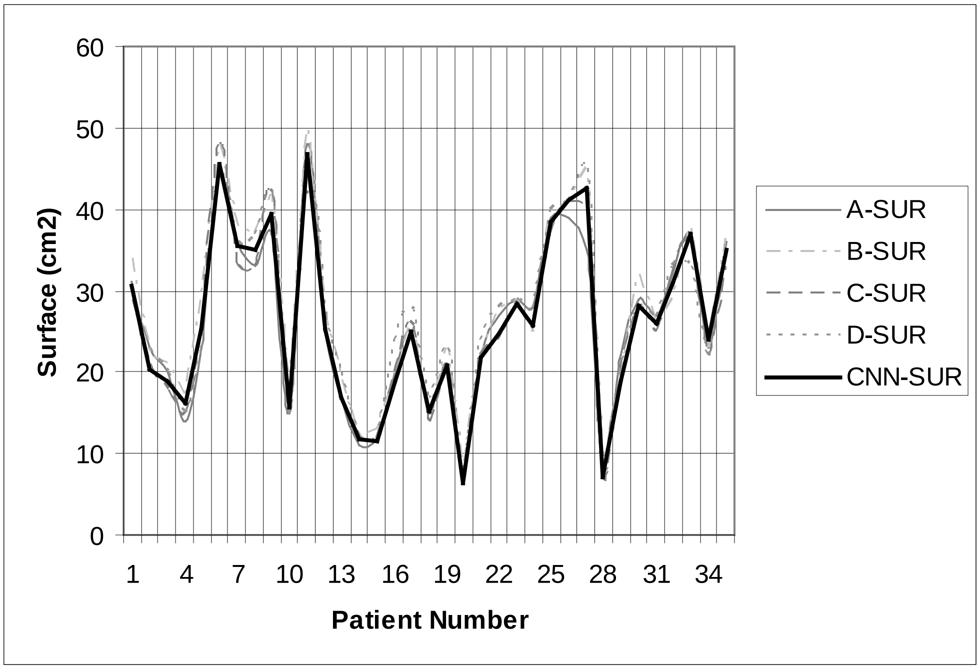

Figure 10. Thyroid surface area (cm^2) calculated by experts {A,B,C,D}and CNN

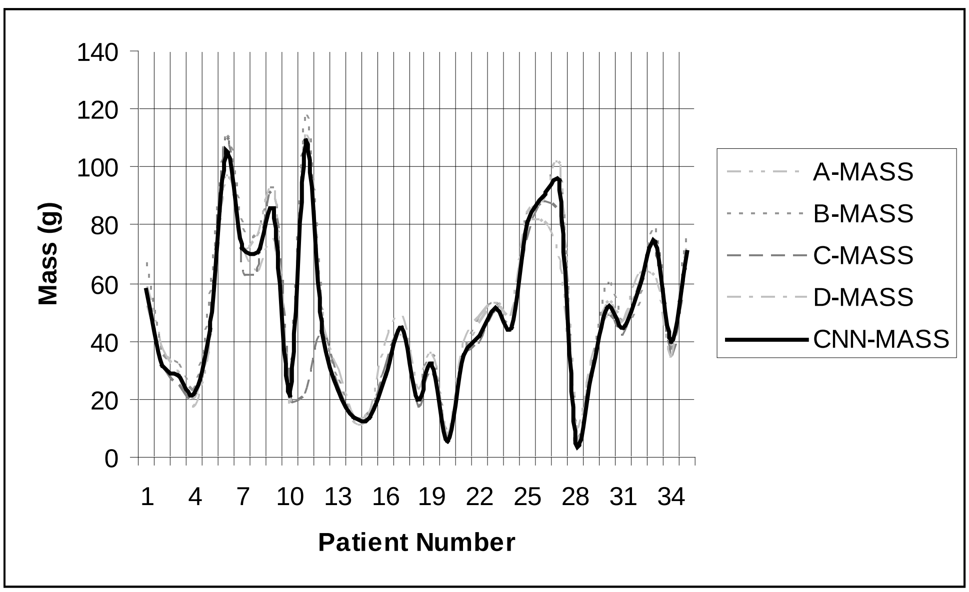

Figure 11. Thyroid Mass (g) calculated by experts {A,B,C,D}and CNN

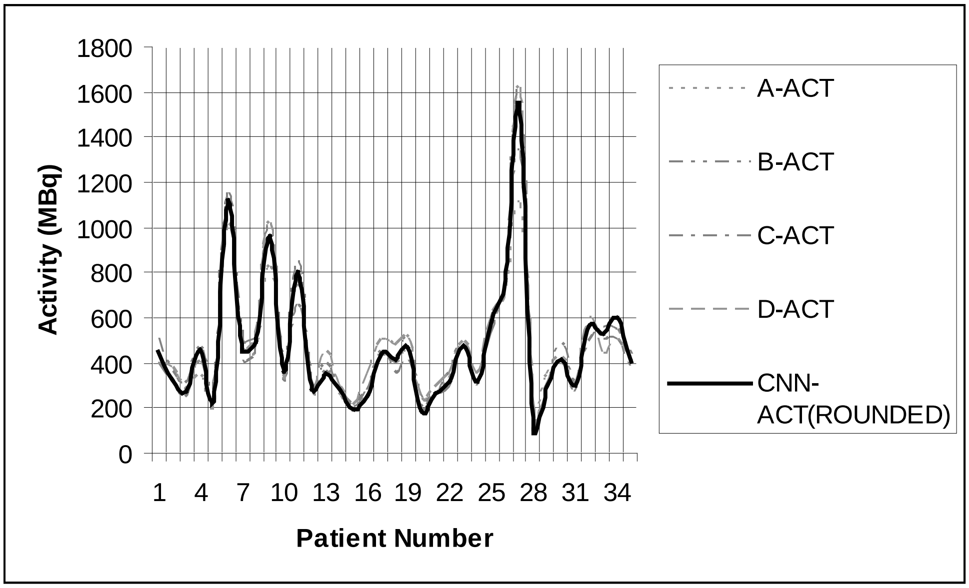

Figure 12. Activity (MBq) calculated by experts {A,B,C,D}and CNN

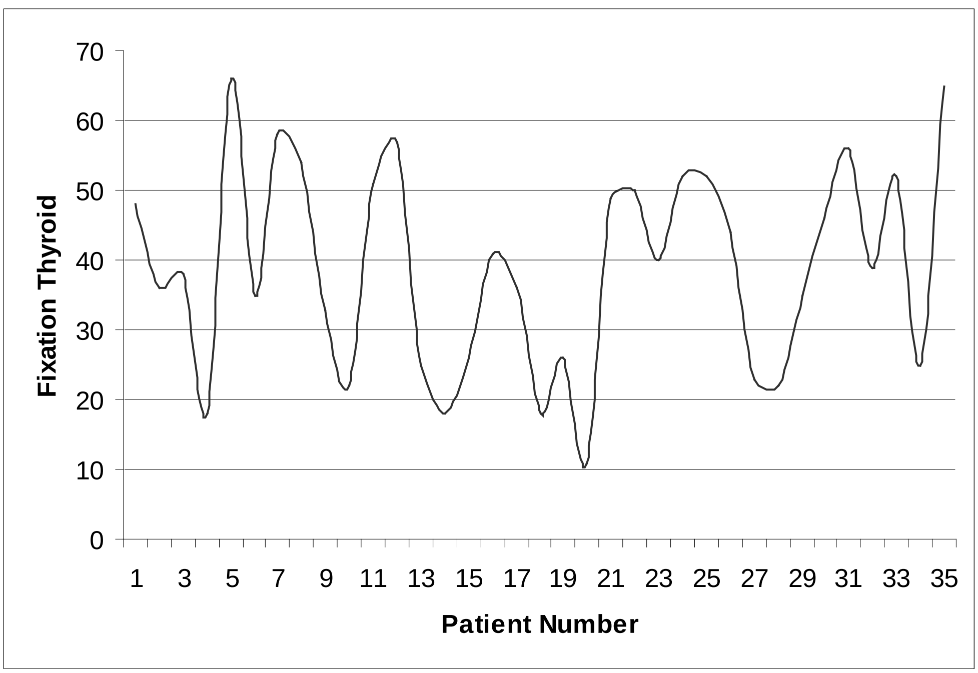

Figure 13. Fixation of thyroid for each patient

Table I. Isocontours obtained manually by experts (A,B,C,D); automatically by CNN approach and calculation of their related parameters (Equations 10-12)

Pat. No	ISOCONTOURS(%)					SURFACE(cm^2)					MASS (g)					ACTIVITY(MBq)					Fix (T)
	A	B	C	D	CNN	A	B	C	D	CNN	A	B	C	D	CNN	A	B	C	D	CNN ROUNDED	
1	28	26	30	30	28.4	31	34	29	29	30.6	59	67	52	52	57,97	451	516	399	399	452	48
2	25	26	28	25	24.1	23	22	21	23	20.3	37	35	31	37	31,31	379	359	318	379	325	36
3	27	25	29	27	26.1	20	21	18	20	18.9	29	32	25	29	27,98	286	312	244	286	275	38
4	33	27	31	30	31.1	14	17	15	15	16.1	17	23	20	20	22,17	341	465	402	402	461	18
5	30	25	28	30	28.6	23	29	25	23	25.6	38	52	41	38	43,61	211	290	230	211	247	66
6	30	28	29	30	28.8	44	48	48	44	45.6	96	110	110	96	105.1	1019	1160	1160	1019	1125	35
7	28	26	30	28	27.7	36	38	33	36	35.5	72	79	64	72	72,17	461	504	411	461	461	58
8	30	27	30	27	28.6	33	37	33	37	35.1	64	76	64	76	70,7	440	521	440	521	490	54
9	33	28	29	30	28.8	37	42	42	42	39.5	74	91	91	91	84.72	826	1023	1023	1023	961	33
10	30	27	30	29	29.4	15	16	15	15	15.6	19	21	19	19	21,03	324	361	324	324	361	22
11	28	27	31	29	29.1	48	50	42	46	46.8	111	118	22	104	109.3	804	858	666	752	802	51
12	28	26	27	26	25.9	25	27	25	27	25.2	41	46	43	46	43,11	268	302	278	302	283	57
13	28	27	28	25	25.6	17	19	17	20	16.9	24	27	24	30	23,6	359	400	359	446	353	25
14	30	28	28	27	28.2	11	12	12	12	11.7	12	13	13	14	13,73	253	276	276	293	286	18
15	29	25	27	26	26.1	12	13	12	12	11.6	13	15	14	15	13,55	186	220	202	209	195	26
16	27	27	27	23	23.9	20	20	20	24	18.9	31	31	31	39	27,93	278	278	278	349	255	41
17	28	27	27	25	25.6	25	26	26	28	25.1	42	44	44	49	445	428	448	448	504	445	36
18	28	27	30	26	27.6	15	15	14	17	15.1	19	19	17	23	19,95	397	397	350	477	415	18
19	29	26	30	26	26.9	21	23	20	23	20.9	31	36	29	36	32,39	442	512	414	512	466	26
20	26	27	29	26	25.6	8	8	7	8	6.4	7	7	6	7	5,5	235	235	194	235	187	11
21	28	28	28	26	26.8	22	22	22	24	21.8	34	34	34	39	34,66	257	257	257	293	265	49
22	26	25	28	25	24.0	27	28	24	28	24.8	46	48	39	48	42,01	337	357	287	357	314	50
23	27	27	28	27	26.8	29	29	28	29	28.3	53	53	50	53	51,31	494	494	466	494	480	40
24	26	28	27	26	25.8	28	25	26	28	25.8	49	43	45	49	44,63	350	303	320	350	321	52
25	28	27	29	27	27.2	39	40	37	40	38.5	80	84	75	84	81,3	568	601	533	601	585	52
26	30	28	28	28	29.2	39	41	41	41	41.2	81	88	88	88	90,17	684	741	741	741	767	44
27	34	30	32	30	32.9	35	45	40	45	42.7	68	100	83	100	95,05	1099	1614	1333	1614	1547	23
28	18	22	28	22	21.2	10	8	7	8	7.0	10	8	6	8	6,3	166	135	102	135	107	22
29	24	28	27	27	25.0	22	19	20	20	18.9	33	28	29	29	27,86	352	300	311	311	298	35
30	27	25	28	28	26.0	29	32	28	28	28.3	53	60	49	49	51,28	425	486	395	395	417	46
31	26	27	28	26	26.3	27	26	25	27	25.9	47	45	42	47	44,84	308	298	275	308	300	56
32	28	30	28	26	27.4	32	29	32	33	30.9	59	52	59	63	58,57	560	490	560	596	562	39
33	26	25	27	29	27.7	37	38	36	33	36.6	74	79	71	62	74	529	559	502	444	529	52
34	24	24	26	26	26.5	23	23	22	22	22.7	37	37	34	34	40	550	550	500	500	599	25
35	25	24	27	25	24.7	36	37	33	36	35.4	72	76	65	72	70,6	408	432	367	408	407	65